J|A|C|S
ARTICLES
Published on Web 05/16/2002

An Approach Based on Quantum Chemistry Calculations and Structural Analysis of a [2Fe-2S*] Ferredoxin That Reveal a Redox-Linked Switch in the Electron-Transfer Process to the Fd-NADP$^+$ Reductase

Renaud Morales,[‡,§] Michel Frey,*[,§] and Jean-Marie Mouesca*[,†]

Contribution from the Service de Chimie Inorganique et Biologique, UMR 5046, DRFMC/CEA-Grenoble, 17 rue des Martyrs, 38041 Grenoble, France, and Laboratoire de Cristallographie et de Cristallogenèse des Protéines, Institut de Biologie Structurale-Jean-Pierre-Ebel CEA-CNRS, 41 Avenue des Martyrs 38027 Grenoble CDX, France

Received July 10, 2001. Revised Manuscript Received December 26, 2001

Abstract: [2Fe-2S*] ferredoxins act as electron carriers in photosynthesis by mediating the transfer of electrons from photosystem I to various enzymes such as ferredoxin:NADP$^+$:reductase (FNR). We have analyzed by density functional theory the possible variations of the electronic properties of the [2Fe-2S*] ferredoxin, from the cyanobacterium *Anabaena*, depending on the redox-linked structural changes observed by X-ray diffraction at atomic resolution (Morales, R.; et al. *Biochemistry* **1999**, *38*, 15764−15773). The present results point out a specific and concerted role of Ser47, Phe65, and Glu94 located at the molecule surface, close to the iron−sulfur cluster. These residues were already known to be crucial for efficient electron transfer to FNR (e.g., Hurley, J. K.; et al. *Biochemistry* **1997**, *36*, 11100−11117). Our calculations suggest that the Glu94 carboxylate negative charge regulates the electron charge delocalization between the Ser47 CO group and the Phe65 aromatic ring, depending on the redox state. The Glu94 carboxylate is stabilized by a strong hydrogen bond implicating a hydroxyl-containing side chain (i.e., Ser or Thr) at location 47. We propose that the Phe65 ring acts as an intermediary carrier receiving the reducing electron prior to its transfer from the reduced Fd to FNR, in view of its central role in the Fd−FNR interaction.

I. Introduction

Plant-type [2Fe-2S*] ferredoxins play a central role as electron carriers in the conversion of light energy into chemical energy by photosynthetic organisms. They mediate the transfer of high-energy electrons, photoproduced by photosystem I (PSI), to various ferredoxin-dependent enzymes such as the FAD flavoenzyme ferredoxin:NADP$^+$:reductase (FNR).[1,2] FNR catalyzes the reduction of NADP$^+$ to NADPH following the reaction 2Fd rd + NADP$^+$ → 2Fd ox + NADPH. NADPH is eventually used to reduce CO_2 to carbohydrates in the Calvin cycle.[3,4] The intra- or intermolecular electron-transfer properties of photosynthetic ferredoxin and FNR have been extensively studied by joint site-specific mutagenesis, biochemical and kinetics measurements (e.g., refs 5−8). More recently, the first three-dimensional crystallographic model of a Fd/FNR complex from the cyanobacterium *Anabaena* has been reported.[9] It appears that the electron transfer from ferredoxin to FNR requires the formation of a specific transient complex between the reduced Fd (Fd rd) and a preformed FNR/NADP$^+$ complex. In short, the interaction between the two molecules involves the shallow concave side of FNR surrounding the solvent-exposed moiety of the FAD isoalloxazine ring, which is the electron acceptor, and the ferredoxin bulge including the [2Fe-2S*] cluster, which is the electron donor (cf. Figure 1a).

Much experimental evidence suggests that, in plant-type ferredoxins, the electron transfer is confined to the [2Fe-2S*] cluster and its immediate environment (cf. Figure 1a). First, ^{57}Fe Mössbauer spectroscopy has shown that both irons are ferric in the oxidized state [2Fe-2S*]$^{2+}$ whereas the reduced state [2Fe-2S*]$^{1+}$ corresponds to a localized mixed-valence

* Authors to whom correspondence should be addressed. E-mail: mouesca@drfmc.ceng.cea.fr, michel.frey@worldonline.fr.
† Service de Chimie Inorganique et Biologique, UMR 5046, DRFMC/CEA-Grenoble.
‡ Present address: Imperial Cancer Research Fund, Clare Hall Labs, Blanche Lane, South Mimms, Herts EN6 3L D, U.K.
§ Institut de Biologie Structurale-Jean-Pierre-Ebel CEA-CNRS.

(1) Knaff, D. B.; Hirasawa, M. *Biochim. Biophys. Acta* **1991**, *1056*, 93−125.
(2) Holden, H. M.; Jacobson, B. L.; Hurley, J. K.; Tollin, G.; Oh, B. H.; SKjeldahl, L.; Cheng, Y. K.; Xia, B.; Markley, J. L. *J. Bioenerg. Biomembr.* **1994**, *26*, 67−88.
(3) Carrillo, N.; Vallejos, R. H. In *Toics in Photosynthesis*; Barber, Ed.; Elsevier: Amsterdam, 1987; Vol. 8, pp 527−560.
(4) Arakaki, A. K.; Ceccarelli, E. A.; Carrillo, N. *Faseb J.* **1997**, *11*, 133−140.
(5) Batie, C. J.; Kamin, H. *J. Biol. Chem.* **1984**, *259*, 11976−11985.
(6) Sancho, J.; Gómez-Moreno, C. *Arch. Biochem. Biophys.* **1991**, *288*, 231−238.
(7) Hurley, J. K.; Weber-Main, A. M.; Stankovich, M. T.; Benning, M. M.; Thoden, J. B.; Vanhooke, J. L.; Holden, H. M.; Chae, Y. K.; Xia, B.; Cheng, H.; Markley, J. L.; Martinez-Julvez, M.; Gómez-Moreno, C.; Schmeits, J. L.; Tollin, G. *Biochemistry* **1997**, *36*, 11100−11117.
(8) Martinez-Julvez, M.; Medina, M.; Hurley, J. K.; Hafezi, R.; Brodie, T. B.; Tollin, G.; Gómez-Moreno, C. *Biochemistry* **1998**, *37*, 13604−13.
(9) Morales, R.; Charon, M.-H.; Kachalova, G.; Serre, L.; Medina, M.; Gómez-Moreno, C.; Frey, M. *Embo Rep.* **2000**, *1*, 271−276.

10.1021/ja011680o CCC: $22.00 **© 2002 American Chemical Society**

Table 1. Biophysical Properties of Selected Mutants of *Anabaena* Ferredoxin PCC7120

	reactivities[a,b] k ($\times 10^{-8}$ M^{-1} s^{-1})	redox potential gradient[a,c] ΔV (mV)	dissociation constant[a] K_d (mM)	stability[d] $\Delta\Delta G'$ (kcal/mol)	PDB code (rms deviation Å)
wild type	1.2 ± 0.1	+81	9.31 ± 0.7		
F65Y	7.3 ± 0.2	nd[e]	nd	-0.2 ± 0.2	
F65W	0.9 ± 0.1	nd	nd	0.1×0.2	
F65I	0.0002	+61	nd	-1.7 ± 0.2	
F65A	0.00007	nd	120 ± 10	-1.4 ± 0.2	
E94K	0.00005	−2	26 ± 3	-0.5 ± 0.2	1J7B (0.40)
E94Q	0.00013	nd	13 ± 4	-0.3 ± 0.3	
E94D	1.3 ± 0.5	nd	nd	-0.8 ± 0.2	
S47A	<0.005	+67	nd		IQOG (0.25)
S47T	0.9 ± 0.1	nd	10.9 ± 0.5		

[a] Taken from refs 7 and 44. [b]Second-order rate constants for oxidation of reduced Fd by oxidized FNR. [c]Redox potential gradients between FNR (semiquinone) and Fd in the complex. [d] $\Delta\Delta G'$= mutant ΔG − wild-type ΔG. Taken from ref 45. [e] nd, not determined.

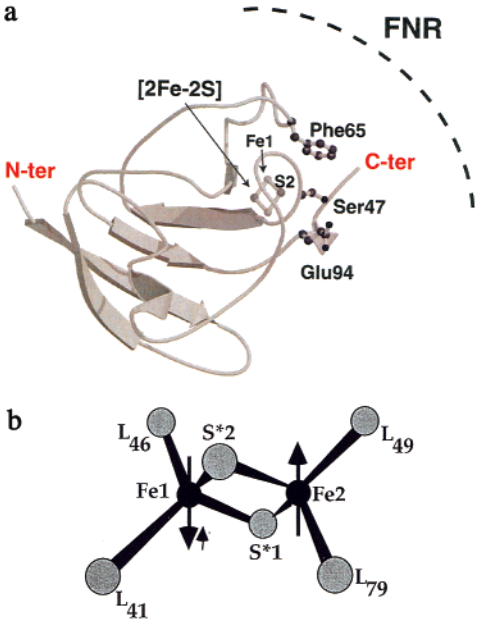

Figure 1. (a, top) Ribbon diagram of the three-dimensional structure of a [2Fe-2S*] plant-type ferredoxin.[43] The protein fold consists of four strands forming a barrel-like structure opposite a protruding zone including the iron−sulfur cluster (represented by a lozenge) and its four cysteic ligands to the protein. The *Anabaena* PCC7119 plant-type ferredoxin contains 98 amino acids. The three labeled residues Phe65, Ser47, and Glu94 are crucial for electron transfer to the ferredoxin functional partner, the ferredoxin NADP$^+$ reductase FNR.[7,9,12] (b, bottom) Schematic diagram of the structure and spin alignment for the $[Fe_2S_2(SL)_4]^{3-}$ reduced form ($S = {}^1/_2$). SL = cysteic ligands.

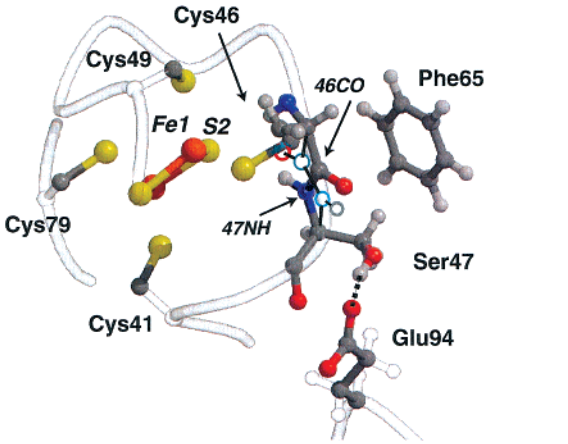

Figure 2. A view of the [2Fe-2S] cluster and its vicinity for the oxidized (OX) and reduced (RD) structures.[13] In RD, 46CO (ball and stick) is pointing away from the [2Fe-2S*] cluster S2 sulfur atom, and the 47NH amide is pointing toward S2, building a NH···S hydrogen bond. In OX, the 46CO (thin line) is pointing toward S2, and 47NH is pointing away from S2. Note that in both conformations the 46−47 peptide link and the Phe65 aromatic ring are nearly stacked onto each other (see also Figure 3). The crucial hydrogen bond between the Ser47 hydroxyl group and the Glu94 carboxylate is represented by a dotted line.

Fe^{2+}/Fe^{3+} state of $S = {}^1/_2$ magnetic ground state (for review, see ref 10). The formal valence state Fe^{2+} has been assigned to the iron ion closest to the molecular surface (labeled Fe1 in the present paper; see Figures 1a, 2, and 3) by temperature-dependent proton NMR experiments.[11] Second, extensive genetics and kinetics studies on *Anabaena* Fd have shown that three residues, Phe65, Glu94, and Ser47, located in the cluster vicinity (Figure 1a) play a crucial *functional* role. Indeed, some of their mutations cause a dramatic decrease of electron transfer to FNR, although the association and redox potential gradients between the two proteins are not significantly altered[7] (Table 1). In other words, to keep the electron-transfer capacity of the ferredoxin/FNR complex, the ferredoxin residue 65 has to be aromatic,[12] residue 94 acidic, and residue 47 a serine or a threonine.[7] Third, comparisons of the oxidized and reduced *Anabaena* Fd crystal structures have revealed that the [2Fe-2S*] cluster binding loop presents a redox-linked conformational "flip" centered on the peptide link 46−47[13] (cf. Figures 2 and 3). Taking into account the results of earlier theoretical calculations[14] yielding computed charge distributions over iron−sulfur clusters, it has been proposed that such a change might be related to a change in net charge of one of the [2Fe-2S*] cluster bridging sulfurs (S2) upon reduction or oxidation.[13]

In the present work, we have analyzed the possible *variations* of the electronic and charge properties of the *Anabaena* PCC7119 ferredoxin [2Fe-2S*] cluster and its immediate environment depending on the redox state of the structure. We have used density functional theory (DFT) calculations and high-resolution X-ray structures of the oxidized and reduced states[13] (PDB 1CZP and 1QT9). In effect, a DFT-based quantum-mechanical code seemed most appropriate to tackle a problem

(10) Beinert, H.; Holm, R. H.; Münck, E. *Science* **1997**, *277*, 653−659.
(11) Dugad, L. B.; LaMar, G. N.; Banci, L.; Bertini, I. *Biochemistry* **1990**, *29*, 2263−2271.
(12) Hurley, J. K.; Cheng, H.; Xia, B.; Markley, J. L.; Medina, M.; Gómez-Moreno, C.; Tollin, G. *J. Am. Chem. Soc.* **1993**, *115*, 11698−11701.
(13) Morales, R.; Charon, M.-H.; Hudry-Clergeon, G.; Pétillot, Y.; Norager, S.; Medina, M.; Frey, M. *Biochemistry* **1999**, *38*, 15764−15773.
(14) Noodleman, L.; Peng, C. Y.; Case, D. A.; Mouesca, J.-M. *Coord. Chem. Rev.* **1995**, *144*, 199−244.

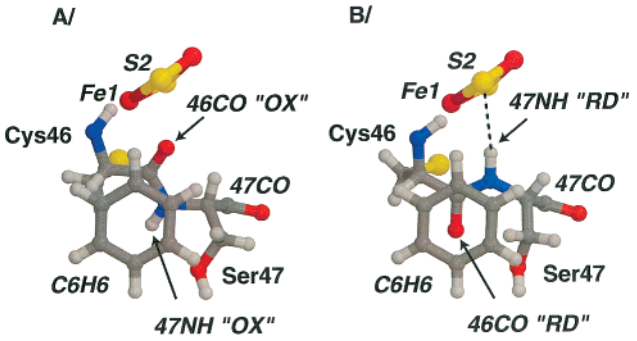

Figure 3. Ferredoxin [2Fe-2S*] cluster and 46−47 peptide redox-linked "flip" seen through the Phe65 ring (in the plane of the figure) in the OX (A) and RD (B) structures. The 47NH···S2 hydrogen bond observed in the RD structure is depicted by a dotted line (B).

consisting of determining electron charge/spin distributions of a biological system counting two high-spin transition metal ions as well as quite a few amino acid residues (the largest calculation performed for this study involved 75 atoms without any molecular symmetry).

In our calculations, we assumed that the solvent effect is similar for the two structural redox states of the ferredoxin, in solution or within the complex. Indeed, in classical electrostatics approaches (e.g., ref 15), the differences in the OX versus RD water molecule patterns, at the protein surface around the above-mentioned 46−47 peptide link, would be smoothed following their replacement by layers of undifferentiated dipoles. Moreover, these few hydrogen-bonded water molecules are neutral. Taken together, this suggests that the differential impact of the OX versus RD solvent patterns on the cluster charge distribution should be minor.

More sophisticated approaches[16−19] couple the cluster, treated by quantum mechanics, with its proteic and solvent environment, treated classically. This allows the solvent reaction field to act back on the cluster charge distribution. In this regard, our work stands as an exploratory step for more complete studies on Fd/FNR electron-transfer problem. However, from our experience,[18] this key improvement in the modeling should not drastically alter the cluster charge distribution though remaining mandatory for the purposes of energetics (i.e., redox potential, pK_a's).

Our major aim was to try to elucidate the role of the critical Phe65, Glu94, and Ser47 residues as well as the functional significance, if possible, of the redox-linked conformational change of the peptide link 46−47.

II. Experimental Procedure

II.1. [2Fe-2S*] Cluster and Its Environment. The high-resolution structures of three oxidized and two reduced ferredoxin molecular models in various crystallographic environments were obtained on the basis of X-ray diffraction data obtained at 1.3 and 1.17 Å resolution, respectively.[13] The accuracy and precision of these models are of the same order of magnitude as those obtained for model compounds.[20] The only significant structural differences between all these models are due to the redox state of the molecules themselves, which mostly pertain to the [2Fe-2S*] cluster and its immediate environment, including the above mentionned 46−47 peptide link.[13]

In the following discussion, oxidized and reduced protein *crystallographic* structures will be referred to by (upper case) "OX" and "RD" labels, respectively, while oxidized (Fe^{3+}-Fe^{3+}) and reduced (Fe^{3+}-Fe^{2+}) *electronic* states will be identified with (lower case) "ox" and "rd" labels. Due to the weak ligand field exerted on the iron d orbitals by the surrounding sulfur ions, the iron atoms present a local high-spin configuration ($S(Fe^{3+}) = {}^5/_2$ and $S(Fe^{2+}) = 2$). Both iron spins are antiferromagnetically coupled, resulting in a total spin of $S = 0$ in the oxidized $[2Fe\text{-}2S^*]^{2+}$ (ox) species and in a total $S = {}^1/_2$ spin state in the reduced $[2Fe\text{-}2S^*]^{1+}$ (rd) species (see Figure 1b).

Pure spin antiferromagnetic species are not directly reachable computationally. One can, however, have recourse to the use of broken-symmetry spin states, corresponding to the assembling of two weakly interacting high-spin [FeS_4] building blocks or monomers. For the reduced 1+ dimer, one would then expect to find an atomic spin population of +5 on one iron site (corresponding to the five unpaired spins of a d^5 Fe^{3+} ion) and a spin population of −4 on the other iron site (corresponding to the four unpaired spins of a d^6 Fe^{2+} ion), resulting in a total spin population of 1 for the whole spin-coupled dimer. In fact, covalency (orbital mixing) between iron and sulfur orbitals reduces those theoretical iron spin populations by a factor of 0.6−0.7, the remaining 30−40% of the spin population being scattered among sulfur and ligand atoms. In our calculations on reduced (1+) dimers, we precisely trace back this scattered spin population, as an index of the way the extra reducing electron is delocalized toward the ligands.

II.2. Modeling of the [2Fe-2S*] Cluster Environment. In our calculations, we have considered the [2Fe-2S*] cluster and selected residues of its immediate environment (cf. Figure 2). We thus included the four cysteine ligands as well as the only residues whose mutations lead to a drastic decrease in the electron-transfer rate to FNR, i.e., Phe65, Ser47, and Glu 94 (cf. Table 1).

We considered [2Fe-2S*] cluster ligands, from simple ones to more elaborate and realistic ones, of the form $[Fe_4S_4(L_{41}L_{46}L_{49}L_{79})]^{2-/3-}$ or simply $[Fe_4S_4(L_k)_4]^{2-/3-}$ ($k = 41, 46, 49, 79$).

We started with a very simple model compound **I**, where all four cysteinyl ligands have been replaced by $(SH)^-$ groups. Compound I has been modeled after the reduced RD geometry. Its only purpose is to illustrate how we will assert the electron-transfer problem in this paper. The results (Table 2a) and corresponding discussion are therefore reported in an Appendix section at the end of this paper.

In compound **II**, we considered the four cysteines, thus setting L equal to $(SCH_2CH(NH_2)COH)^-$, for both RD and OX geometries.

In compound **III**, the previous model has been simplified by keeping only $L_{46} = (SCH_2CH(NH_2)COH)^-$ while replacing the three other ligands by simpler $(SH)^-$ groups.

Finally, in compound **IV**, we extended L_{46} to include the next Ser47, thus newly defining L_{46} as $(SCH_2CH(NH_2)CONHCH(CH_2OH)COH)^-$. We further included the Glu94 residue.

From the start, we included in our calculations the Phe65 aromatic ring in view of its crucial structural[9] and functional[12] role in electron transfer from Fd to FNR. We modeled Phe65 as a phenyl ring C_6H_6 according to the RD and OX original structures. Furthermore, we modeled the Glu94 residue as a charged $(CH_3COO)^-$ group.

Moreover, we also decided to compute the electronically reduced (rd) state for the four oxidized (OX) structural model compounds **I**−**IV** (as well as reversibly, the oxidized (ox) state for the four reduced (RD) models: not reported). Thus, by "cross-checking" both electronic states and crystallographic structures, we aimed to point out which differential structural features (atoms, residues) are more specifically implicated in the electron-transfer variations to Phe65.

II.3. Quantum Mechanical (QM) Code. All the calculations make use of the Amsterdam LCAO density functional programs (ADF 2.3)

(15) Stephens, P. J.; Jollie, D. R.; Warshel, A. *Chem. Rev.* **1996**, *96*, 2491−2513.
(16) Tannor, D. J.; Marten, B.; Murphy, R.; Friesner, R. A.; Sitkoff, D.; Nicholls, A.; Ringnalda, M.; Goddard, W. A., III; Honig, B. *J. Am. Chem. Soc.* **1994**, *116*, 11875−11882.
(17) Chen, J. L.; Noodleman, L.; Case, D. A.; Bashford, D. *J. Phys. Chem.* **1994**, *98*, 11059.
(18) Mouesca, J.-M.; Chen, J. L.; Noodleman, L.; Bashford, D.; Case, D. A. *J. Am. Chem. Soc.* **1994**, *116*, 11898−11914.
(19) Lovell, T.; Li, J.; Noodleman, L. *Inorg. Chem.* **2001**, *40*, 5267−5278.
(20) Mayerle, J. J.; Denmark, S. E.; DePamphilis, B. V.; Ibers, J. A.; Holm, R. H. *J. Am. Chem. Soc.* **1975**, *97*, 1032.

Table 2. Spin (Index *S*) and Charge (Index *Q*) Population Distribution for Some Atoms and Groups of Compounds **I** and **II**[a]

(a) Compound **I**

	−Phe65			+Phe65		
(I) RD	ox	rd1	rd2	ox	ex30	ex21
Fe1	3.259	2.794	−3.225	3.258	2.757	3.406
Fe2	−3.206	−3.226	2.684	−3.197	−3.239	−3.220
$\sum_S$ Phe				−0.012	0.078	0.922
$\sum_Q$ Phe				0.018	0.080	0.924
HOMO2	0	0	0	0	0	1
HOMO1	0	1	1	0	1	0
R[b]				0	0.233	3.049
energy	−44.818	−30.673	−39.562	−118.421	−112.340	−113.026

(b) Compound **II**

	−Phe65			+Phe65		
(Cys)×4 RD	ox	rd1	rd2	ox	ex30	ex21
Fe1	3.207	3.031	3.213	3.207	2.875	3.378
Fe2	−3.144	−3.165	−2.957	−3.144	−3.166	−3.148
$\sum_S$ CO41	0.002	−0.061	0.081	0.002	−0.054	−0.001
$\sum_S$ CO46	0.008	−0.120	0.153	0.008	−0.012	−0.017
$\sum_S$ CO49	−0.016	−0.152	−0.133	−0.016	−0.076	−0.044
$\sum_S$ CO79	−0.017	−0.158	−0.102	−0.017	−0.172	−0.039
$\sum_S$ Phe				∼0	∼0	−0.946
$\sum_Q$ Phe				−0.021	−0.022	−0.967
HOMO2	0	0	0	0	0	1
HOMO1	0	1	1	0	1	0
energy	−288.214	−284.526	−284.471	−361.772	−357.683	−355.900

[a] In the absence (−Phe65) or in the presence (+Phe65) of the Phe65 phenyl ring, for the redox states ox, rd1 (reducing electron on Fe1) and rd2 (reducing electron on Fe2) and for the reduced ex30/ex21 states (see main text). The energies are reported in eV. [b] See Appendix.

developed by Baerends and co-workers.[21−26] We considered there only the potential referred to as "VBP" (Vosko, Wilk, and Nusair's exchange and correlation energy[27,28] completed by nonlocal gradient corrections to the exchange by Becke[29] and to the correlation by Perdew[30]). We used triple-ζ (plus polarization) basis sets for all atoms.

For most of the calculations, we encountered convergence difficulties due to the competition between two (quasi-) degenerate and oscillating orbitals. We had recourse to an ADF-specific mixing option, introducing fractional molecular orbital occupations when convergence is difficult to achieve by other means (a standard QM computation operates with integer occupation numbers). This option proceeds by mixing the characters of the two oscillating orbitals, bringing artificially their energy difference to nearly zero. However, the correct description of the original orbitals can be then regained by a one-cycle run with integer occupation numbers and the mixing option turned off. We thus do not obtain a "real" state, but rather a mix of two states that, if one allows orbital relaxation (the one-cycle procedure prevents it), are individually unreachable (at least in all our attempts) by the usual DFT means. These "mixed" (and, by construction, unrealistic) states will not be presented in the following Tables 2 and 3.

The label "HOMO" and "LUMO" refer to "highest occupied molecular orbital" and "lowest unoccupied molecular orbital", respectively.

II.4. Concepts and QM Technicalities. This paper deals with electron transfer, more precisely, with some aspects of it related to the so-called "nuclear factor" (energy matching of the electronic orbitals of a donor D and an acceptor A) and to the so-called "electronic factor" (overlap of the electronic wave functions of the donor and acceptor). We will not consider anything pertaining to transition states. In our investigations, the donor will be the [2Fe-2S*] anion in the reduced (1+) state. We do not specify yet the nature of the acceptor orbital as this depends on the presence/absence of the Phe65 amino acid ring.

Let Φ_D and Φ_A be the orbitals involved in the electron-transfer process, localized on D and A, respectively, and let $S_{DA} = <\Phi_D|\Phi_A>$ be their mutual overlap. These local orbitals can be obtained, for example, by separately converging both the A and D electronic states. In the combined [D−A] system, both Φ_D and Φ_A interact to build the two molecular orbitals $\{\Psi_\pm\}$.

In the cases encountered here, the two local orbitals Φ_D and Φ_A are quasi- (but not exactly) degenerate. When both the D and A local orbitals present no orbital interaction at all ($S_{DA} = 0$), and since the probability of transfer from D to A is proportional to S_{DA}^2, there is obviously no transfer possible from D to A (the distance between the respective geometrical centers of both D and A molecules is moreover ∼8.22 Å when [A] = [C_6H_6]). The mixed state we converge stands therefore as a *physical* equal mixing of both local orbitals.

In all biologically relevant cases encountered in this study (**III**, **IV**), the interaction is rather weak ($S_{DA}^2 \ll 1$). As a consequence, the resulting molecular orbitals Ψ_+ and Ψ_- are best described within a valence bond framework by

$$\begin{cases}\Psi_+ \approx \Phi_D - (S_{DA}/2)\Phi_A \\ \Psi_- \approx \Phi_A - (S_{DA}/2)\Phi_D\end{cases} \Leftrightarrow \begin{cases}\Phi_D \approx \Psi_+ + (S_{DA}/2)\Psi_- \\ \Phi_A \approx \Psi_- + (S_{DA}/2)\Psi_+\end{cases} \quad (1)$$

with $\langle\Psi_+|\Psi_-\rangle = 0$. As it turns out, the Ψ_+ molecular orbital is mainly localized on the Fe1 d orbital while Ψ_- is rather centered around the phenyl ring orbital. Let us call Δ the energy gap between the HOMO Ψ_+ and the LUMO Ψ_- (Δ is proportional to S_{DA}).

When both local D and A orbitals are interacting ($S_{AD} \neq 0$), one would like to "quantify" somehow the amount of interaction. One simple way consists of ascribing 0.5 to each molecular orbital Ψ_+ and Ψ_- and converging that state in order to measure directly their mutual energy gap Δ. But convergence could not be systematically achieved for this last electronic state. We can still consider the fractional

(21) Baerends, E. J.; Ellis, D. E.; Ros, P. *Chem. Phys.* **1973**, *2*, 41−51.
(22) Baerends, E. J.; Ros, P. *Chem. Phys.* **1973**, *2*, 52−59.
(23) Baerends, E. J.; Ros, P. *Int. J. Quantum Chem., Quantum Chem. Symp.* **1978**, *12*, 169−190.
(24) Bickelhaupt, F. M.; Baerends, E. J.; Ravenek, W. *Inorg. Chem.* **1990**, *29*, 350−354.
(25) Ziegler, T. *Chem. Rev.* **1991**, *91*, 651−667.
(26) TeVelde, G.; Baerends, E. J. *J. Comput. Phys.* **1992**, *99*, 84−98.
(27) Vosko, S. H.; Wilk, L.; Nusair, M. *Can. J. Phys.* **1980**, *58*, 1200.
(28) Painter, G. S. *Phys. Rev.* **1981**, *B24*, 4264−4270.
(29) Becke, A. D. *Phys. Rev.* **1988**, *A38*, 3098−3100.
(30) Perdew, J. P. *Phys. Rev.* **1986**, *B33*, 8822−8824.

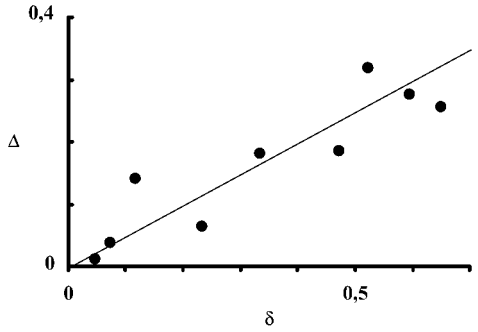

Figure 4. Plot of Δ (eV), energetic gap between the HOMO/LUMO molecular orbitals resulting from the interaction of the electron donor (Φ_D) and acceptor (Φ_A) valence bond orbitals (see eq 1), as a function of δ, spin population (fractional occupation number) difference of the two partially occupied molecular orbitals in the artificial mixed state (see text).

occupation numbers in the artificial mixed state. The spin population difference δ of the two partially occupied molecular orbitals is expected to be about zero for noninteracting D and A orbitals, whereas this difference increases with Δ. Anticipating our computational results presented in the section III, we plotted δ as a function of Δ in Figure 4. The expected linearity is satisfyingly realized.

We also computed excited states resulting from a one-cycle calculation reaffecting integer (0 or 1) occupations to the two originally mixed (fractionally occupied) HOMO molecular orbitals Ψ_+ or Ψ_-, at the price, however, of not allowing orbital relaxation (that last effect being precisely at the source of our convergence problems). This procedure still helps to visualize, through their spin population distribution, these two molecular orbitals.

Let us call "ex30" and "ex21" the two states having the following molecular orbital occupations $(\Psi_+)^1(\Psi_-)^0$ and $(\Psi_+)^0(\Psi_-)^1$, respectively. The first excited state "ex30" can be ideally described as $[Fe_2S_2]^{1+}$-$[A]^0$ (no charge transfer from the [2Fe-2S*] "rd" core to the acceptor), the other one "ex21" by $[Fe_2S_2]^{2+}[A]^{1-}$ (one-electron transfer leaving a [2Fe-2S*] "ox" core and charged acceptor).

III. Results

III.1. The Case of Compound II. In the first series of calculations, we considered the $[Fe_2S_2(Cys)_4]^{2-/3-}$ compound **II**, with or without the Phe65 ring, in the RD crystallographic structure (cf. Table 2b). We there reported in detail the spin populations obtained for the CO groups of the four cysteines. A few points should be noted.

First, in the absence of the ring, about half of the reducing electron delocalizes itself onto the four cysteic CO groups (under "rd1"). The iron and CO orbitals are mixed in the molecular orbital receiving the extra electron. Notice in particular that the Fe1 spin population (3.03) is correspondingly larger than that of a typical high-spin ferrous ion (2.7). The same delocalization phenomenon occurs when the extra electron is forced to be on the other Fe2 monomer (under "rd2"). This delocalization is roughly equally mediated from whichever of the iron sites to the carbonyl groups via the Sγ cysteic sulfur atoms. The energy difference between both electronic configurations rd1 and rd2 leans only slightly in favor of the former one by 0.06 eV, as was already the case with simple (SH) peripheral ligands.

Second, and now in the presence of the ring, the previously described electron spin population delocalization still occurs. However, the CO46 group finds itself depleted, by a factor 10, from most of its former charge due to the presence of the phenyl ring onto which it is nearly perfectly stacked (see Figure 3B), when comparing both the "rd1" and "ex30" electronic structures. By contrast, CO41 and CO79 spin populations are unaffected (that of CO49 being cut by half). The four CO groups are unequally affected by the depletion. The Fe1 becomes more "ferrous-like" in the process. Considering further the "ex21" electronic state, it can be seen that the reducing electron is now essentially localized on the phenyl ring, with little spin left on the CO groups. It has not been possible to compute the molecular orbital energy-based quantity Δ (cf. section II.4) because of convergence problems, but the corresponding molecular orbital population-based quantity δ, here 0.264, points toward a rather large overlap of the donor and acceptor molecular orbitals.

Finally, at this level of modeling of the donor system, the same set of observations can be made when the crystallographic reduced RD structure is replaced by the oxidized one OX. It should be noted that the CO46 group, though stacked somewhat aside from the C_6H_6 ring (see Figure 3A) in the OX structure, still allows for orbital interactions between the carbonyl and phenyl groups.

III.2. The Case of Compound III. For the sake of simplification, we then replaced the (Cys41), (Cys49), and (Cys79) residues by (SH) ligands, while keeping intact the (Cys46) group (**III**), only to realize that the previous results (cf. section III.1) are unaffected by this drastic substitution (cf. Table 3, under the heading "Cys46"). This allowed us to speed somewhat the computational part of our work by adding other residues (see below) without keeping those which do not play any significant role in the electron process under study. The quantity Δ was then found to be 0.14 eV using the RD structure and 0.19 eV using the OX one (the difference being insignificant). These values point again toward a fairly good orbital interaction between the CO46 and phenyl groups whatever the redox state. In addition, as shown in Table 3a (OX) and 3b (RD), the CO46 groups are again depleted from their spin populations (computed to be about −0.2 in the absence of Phe65: not reported). Notice moreover that, for the reduced "ex30" state in the OX structure, a significant amount of charge (−0.17) is delocalized onto the phenyl ring, in contrast to the RD case, where the whole reducing electron is strictly localized on Fe1, thus bearing a typically ferrous-like spin population of 2.73.

III.3. The Case of Compound IV. In the next series of calculations, we considered the $[Fe_2S_2(SH)_3(Cys46-Ser47)]^{2-/3-}$ compound **IV**, again with or without the Phe65 ring (cf. Table 3a for the OX structure and Table 3b for the RD structure, under the heading "Cys46 + Ser47"). We first aimed at a better description of the NH47···S2 hydrogen bond, especially as this may affect the way the CO46 "flip" between RD and OX structures is taken into account in our computations (see Figure 3). The following results, pertaining to the "sink" role of the CO47 group, thus came as a surprise.

In effect, it can be first seen from our results that the CO47 group now replaces the CO46 one in terms of the amount of spin population born (around −0.35/−0.38 in the "ex30" redox state) in the presence of Phe65. This translates a relatively better stabilization of the CO47 orbitals with respect to the CO46 ones, now pushed up in energy, most probably due to the different local environment of each (cysteic and seric) carbonyl group. This important CO47 spin population is present despite the near phenyl group, in contrast to the depletion previously described when only CO46 is considered.

Table 3. Spin (Index *S*) Population Distribution for Some Atoms and Groups of Compounds **III** (Cys46) and **IV** (Cys46 + Ser47 and Cys46 + Ser47 + Glu94), in the Presence of the Phe65 Phenyl Ring, for the Reduced ex30/ex21 States (See Main Text)[a]

(a) The OX Crystallographic Structure

	Cys46		Cys46 + Ser47		Cys46 + Ser47 + Glu94	
OX	ex30	ex21	ex30	ex21	ex30	ex21
Fe1	2.845	3.261	3.069	3.161	2.661	3.360
Fe2	−3.191	−3.178	−3.186	−3.181	−3.196	−3.173
$\sum_S$ CO46	−0.063	−0.008	0	0	0	0
$\sum_S$ CO47			−0.378	−0.036	−0.007	−0.418
$\sum_S$ Phe65	−0.170	−0.813	−0.065	−0.737	−0.994	−0.491
HOMO2	0	1	0	1	0	1
HOMO1	1	0	1	0	1	0
energy	−183.174	−182.924	−249.291	−248.621	−285.534	−285.797

(b) The RD Crystallographic Structure

	Cys46		Cys46 + Ser47		Cys46 + Ser47 + Glu94	
RD	ex30	ex21	ex30	ex21	ex30	ex21
Fe1	2.732	3.446	3.086	3.242	2.825	3.417
Fe2	−3.226	−3.205	−3.224	−3.218	−3.224	−3.207
$\sum_S$ CO46	−0.020	−0.020	0	0	0	0
$\sum_S$ CO47			−0.352	−0.027	−0.107	−0.010
$\sum_S$ Phe65	−0.003	−0.955	−0.169	−0.753	−0.056	−0.938
HOMO2	0	1	0	1	0	1
HOMO1	1	0	1	0	1	0
energy	−182.827	−182.156	−249.789	−248.786	−286.457	−284.902

[a] The energies are reported in eV.

Table 4. Charges *Q*, Energies *E*, and Iron Spin Populations for the Isolated Donor (D) and Acceptor (A) Molecules and for the Combined [D−A] System[a]

D: [2Fe–2S*] (L = SH)				A: phenyl		[D–A]	
Q_D	E_D (eV)	Fe1	Fe2	Q_A	E_A (eV)	*R* (eV)	$E_D + E_A + R$
−3	−39.673	2.794	3.226	0	−73.639	−0.080	−113.392
−2.75	−41.374	2.968	3.236	−0.25	−73.786	1.082	−114.078
−2.5	−42.787	3.096	**3.233**	−0.5	−73.689	2.029	−114.357
−2.25	−43.943	3.190	3.223	−0.75	−73.051	2.762	−114.232
−2	−44.818	3.259	3.206	−1	−72.179	3.251	−113.746

[a] The electrostatic energy *R* was defined in the Appendix.

Second, in the case of the "ex21" states for both RD and OX structures, "only" 75% of the charge localizes itself on the phenyl ring. No Δ value, now quantifying the (Fe−CO47)−(C_6H_6) interaction, could be obtained, but the corresponding δ ones are relatively small (0.23 and 0.10 for the RD and OX structures, respectively).

Finally, the most important result, at this step of our computations, is that nothing really dramatic, be it in terms of spin or charge population distributions, seems to distinguish both RD and OX crystallographic structures. CO47 acts in both cases as an electron "sink". This prompted us to include the nearby hydrogen-bonded Glu94 residue in our computations, modeled as a (CH_3COO^-) charged group at the crystallographic RD and OX positions. The results pertaining to the effects of this last inclusion appear in the last colums of Table 3.

Considering first the RD structure, it can be seen that, in the presence of Glu94, most of the "ex30" spin population distribution initially present on the CO47 group disappears in favor of Fe1. The charged Glu94 thus seems to "push" the reducing electron back to the iron site. In the "ex21" state, the phenyl ring receives 94% of the reducing electron. The quantity δ is computed to be 0.23 for the RD structure. For the OX structure, the consequences of the introduction of the Glu94 are drastically different. In effect, the relocalization of the reducing electron onto Fe1 is even stronger in the "ex30" state as no spin population is left on CO47. Such is not the case for the "ex21" state. The reducing electron is there shared almost equally by the CO47 and the phenyl ring (49%). The quantity δ is again computed to be 0.23 for that OX structure. Therefore, in the RD structure, the Glu94 serves as a differential agent in the determination of the reducing electron spin/charge distribution in both crystallographic structures. Both Ser47 (a "sink") and Glu94 (a "trigger") seem therefore to act in a concerted way during the electron-transfer process.

A final point has to be mentioned here, concerning the charges computed on the sulfur bridging ions. We systematically found the charge of the inorganic S2 ion to be more negative than that of S1 by at least 0.1 electron (on average −0.25 versus −0.35 for the "ex30" state, and −0.18 versus −0.28 for the "ex21" state). It is tempting at this stage to link that charge variation on S2 with the 46−47 peptide link "flip". In the RD structure, S2, which is more negatively charged, interacts with NH47 through a hydrogen bond whereas CO46 points away from the cluster and into the solvent. In the OX structure, the reverse is true; that is, the CO46 points toward the less charged cluster S2 atom and NH47 into the solvent (Figures 2 and 3).

IV. Discussion

IV.1. The [2Fe-2S*] Cluster Geometry and Its Environment. The ferredoxin [2Fe-2S*] cluster shows a distorted D_{2h} symmetry in contrast with that of model compounds.[20] More precisely, the Fe1−S* (S*, cluster bridging sulfur) distances and the S*−Fe1−S* angle are respectively longer and smaller than those observed for model compounds whereas the Fe2−S* distances and S*−Fe2−S* angles are nearly the same. This geometrical arrangement is most probably due to the asymmetric distribution of the NH···S bonds around the cluster since those involving the S1−Fe1−S2 moiety, closer to the molecular surface, outnumber those involving the S1−Fe2−S2 "buried" moiety.[13] Moreover, the Fe−S* and Fe−Sγ (Sγ, cysteic sulfur

ligands) are longer in the reduced state by only 0.02 Å at most. Therefore, it has been inferred that the relative elongation of the S1−Fe1−S2 moiety in the oxidized state could help in accommodating the charge density increase due to reduction.[13] Our present computational work shows, from the respective bonding energies calculated when the extra reducing electron is located either on Fe1 or Fe2, that the former iron site 1 is only slightly energetically favored (0.1 eV at the most: cf. Table 2). Therefore, the localization of the reducing electron on Fe1 may also depend on other environmental factors, not taken into account in our model compounds.

IV.2. Cysteines and Their Carbonyl Groups. X-ray and kinetics studies of the serine mutants of the cysteic ligands have shown that their structural and electron-transfer properties are similar to those of the wild-type ferredoxin. This suggested that the cysteine sulfur d orbitals are not required for electron transfer and that the role of the cysteines is merely to stabilize the structure of the [2Fe-2S*] cluster.[31] As already known,[14] our calculations confirm that a significant electron population is delocalized toward the cysteic and cluster bridging sulfur atoms. The surprise came, however, from the fact that the cysteic main-chain carbonyl CO groups also bear a significant amount of the reducing electron population. In this context, the polarized cysteic 3p orbitals serve as mediators of the charge from the iron atom to the carbonyl groups.

IV.3. Phe65 as an Electron Sink. The strict requirement of an aromatic residue at the Fd position 65 for efficient electron transfer to FNR in *Anabaena* obviously prompts either one of the two nonmutually exclusive remarks: the steric properties of an aromatic ring are essential for the formation of a geometrically appropriate functional complex or the ring π orbitals play a determinant role in the electron-transfer process.[12,32,33] The introduction of a C_6H_6 ring in our present models **II**−**IV** has resulted in the delocalization of a fair fraction of the electron population onto the ring for the two crystallographic (RD and OX) structures.

In addition, when Glu94 is taken into account in the calculations, it appears that the phenyl ring charge population in the reduced (RD) structure is nearly twice as large as that of the oxidized (OX) structure. First, this supports the role of Phe65 as a sink for the additional electron population in the protein RD state. Putting aside the switch effect of Glu94, which will be discussed below, this last point is not surprising. Indeed, in the RD structure, CO46 is nearly perfectly stacked onto the Phe65 aromatic ring (Figure 3). Second, this suggests that, again in the presence of Glu94, the nearly perfect stacking of CO46 onto the phenyl ring in the RD structure is most probably the decisive structural factor facilitating electron delocalization toward Phe65, in contrast with the case of the OX structure where CO46 is "only" stacked aside the ring (see Figure 3).

IV.4. Glu94 and Ser47 Switching the Electron in and out of the CO47 Intermediary Electron Reservoir. Kinetic studies involving mutants of Glu94 or its structural neighbors Glu95, T48, and Ser47 have strongly suggested that *both* a negative charge at location 94 and a serine or a threonine at location 47 are essential for a productive electron-transfer complex with FNR (e.g., ref 7). The strict requirement of a glutamic or aspartic residue at location 94 is all the more intriguing as this residue is not located in the immediate vicinity of the [2Fe-2S*] cluster or Phe65, but lies at the periphery of the interaction site with FNR in the crystallographic complex.[9] Actually, the present DFT calculations reveal that a negative charge at location 94 is a prerequisite to differentiate the amount of Phe65 total charge between the RD and OX structures. The sole introduction of a negative charge at location 94 causes, in the reduced RD state, a dramatic "increase" of the Phe65 aromatic ring electron population and, in the oxidized (OX) state, a corresponding "decrease" in favor of the CO47 group, acting as an intermediary reservoir. This suggests that Glu94, in concert with CO47, acts as an electrostatic switch discriminating between the two structural redox states of the protein. It is of interest to note that our calculations show that the replacement of the Glu94 by a positively charged Gln causes the reducing electron to go to the carboxamine group rather than to the phenyl ring (not reported). This last result perfectly explains the total inefficiency of the Glu94Gln mutant in the electron-transfer process whereas the stereochemistry of the Gln94 side chain is probably very close to that of Glu94 in the wild-type enzyme.

Even more intriguing is the strict requirement of a serine or a threonine at location 47 as evidenced by the dramatic impairment of the electron-transfer properties of the Ser47Ala mutant.[7] It has been proposed that this impairment could be structurally related to the lack of a hydrogen bond, present in the wild-type enzyme, between the mutant 47 side chain (Ala) and the carboxylate of residue94 (Glu or Asp).[7] The present DFT calculations do not show any major involvement of the residue47 side-chain hydroxyl, in itself or hydrogen bonded to the residue94 carboxylate, in the electronic distribution in both ferredoxin RD and OX structures. Moreover, in contrast to Glu94, Ser47 is not directly involved in the interaction between Fd and FNR in the crystallographic complex.[9] This leads us to propose that the role of the Ser47 hydroxyl−Glu94 carboxylate hydrogen bond is to hold the Glu94 carboxylate negative charge at a precise spatial location, thus acting as a kind of electrostatic "lasso".

IV.5. Interaction with FNR. Genetic and kinetics experiments[12] as well as the determination of the crystallographic Fd/FNR complex[9] have suggested that the Fd Phe65 aromatic ring π orbitals are involved in the electronic coupling between the two respective prosthetic groups, i.e., the Fd [2Fe-2S*] cluster, the electron donor, and the FNR−FAD isoalloxazine, the electron acceptor. It is very tempting to relate the role of Phe65 as an electron sink for the reduced Fd to its location at the core of the interface between Fd and FNR in the crystallographic complex. Along the same lines, it should be pointed out the Phe65 π orbitals are sufficiently spatially extended to overlap with those of the FNR isoalloxazine, for a wide range of relative orientations of Fd with respect to FNR. This goes along with a flexible mode of "productive" docking of Fd onto FNR which is required for a rapid turnover.[9]

Fd Glu94 is hydrogen bonded to the FNR Lys75 in the crystallographic complex.[9] Steady-state and fast transient kinetics studies of intermolecular electron transfer involving several FNR Lys75 mutants (Arg, Gln, Ser, Glu) have established that

(31) Hurley, J. K.; Weber-Main, A. M.; Hodges, A. E.; Stankovich, M. T.; Benning, M. M.; Holden, H. M.; Cheng, H.; Xia, B.; Markley, J. L.; Genzor, C.; Gómez-Moreno, C.; Hafezi, R.; Tollin, G. *Biochemistry* **1997**, *36*, 15109−15117.
(32) Hurley, J. K.; Salamon, Z.; Meyer, T. E.; Fitch, J. C.; Cusanovich, M. A.; Markley, J. L.; Cheng, H.; Xia, B.; Chae, Y. K.; Medina, M. *Biochemistry* **1993**, *32*, 9346−9354.
(33) Schmitz, S.; Navarro, F.; Kutzki, C. K.; Florencio, F. J.; Bohme, H. *Biochim. Biophys. Acta* **1996**, *1277*, 135−140.

the presence of positively charged side chain (i.e., lysine or arginine) at FNR location 75 is crucial for the stability of an efficient intermolecular Fd/FNR electron-transfer complex.[8] In addition, the interaction between the Lys75Glu FNR mutant and the Fd Glu94Lys mutant does not yield positive results (Hurley, J. K.; Tollin, G., personal communication). This again emphasizes the importance of a distinct location for the negatively charged Glu94 side-chain carboxylate.

IV.6. Other Systems. Genetics, spectroscopic, and biochemical studies suggest that the presence of an acidic residue at location 94 (or equivalent) in various plant-type ferredoxins is also critical for an efficient electron transfer or enzymatic activity for such different partners as FNRs,[34] glutamate synthases,[33,35,36] mitrate and nitrite reductases,[37] or thioredoxin reductases.[38] In all cases there is a serine at location 47 (or equivalent). The few experiments concerning Phe65 (or equivalent) mutants[35,37] show that an aromatic residue at this location is also important, although less critical that Glu94, for optimal electron transfer.

Of particular interest is adrenodoxin (Adx, ref 39; PDB 1AYF), a [2Fe-2S*] cluster-containing enzyme involved in steroid hormone biosynthesis. It has already been observed that the respective oxidized Adx and Fd [2Fe-2S*] clusters and their four cysteic ligands show a similar spatial arrangement in that the OX-Fd CO46 and the Adx CO52 are pointing toward one cluster sulfur atom in the oxidized structures.[13] Superposition of the two structures also shows that Adx Met77 occupies the same spatial location as Fd Phe65. We propose that the Adx Met77 sulfur and the Fd phenyl aromatic ring play the same transitory role in electron transfer since the relatively larger diffusiveness of the sulfur Met 3p orbitals could act similarly to the more extended carbon Phe 2p ring orbitals. However, we have to keep in mind that the direction of the electron flow in Adx is *from* the (NADPH) reductase to the cytochromes P450 whereas in Fd transfer this direction is from PSI *to* the $NADP^+$ reductase.

The redox-linked flip of the 46−47 peptide link[13] seems to serve as a remarkably simple device whose effect on the electron transfer is only operative in the presence of the Glu94 carboxylate. Further studies of this mechanism would be very interesting to pursue, the more so because the same redox flip has also been observed in flavodoxins for which it stabilizes the flavin semiquinone interaction with the protein.[40]

The figures were made with MOLSCRIPT[41] and Raster3D[42] using the Protein Data bank (http://www.rcsb.org/pdb/) atomic coordinates files of the oxidized (1QT9) and reduced (1CZP) structures.[13]

Abbreviations: FNR, ferredoxin-$NADP^+$ reductase; Fd, ferredoxin from *Anabaena* PCC7119 or the identical PCC7120; rd and ox, reduced and oxidized electronic states; RD and OX, reduced and oxidized crystallographic structures; PDB, Protein Data Bank; DFT, density functional theory.

Acknowledgment. We acknowledge the contribution of Dr. Marie-Hélène Charon to the crystallographic studies. We are also indebted to Pr. Carlos Gomez-Moreno and Dr. Milagros Medina from the University of Zaragoza in Spain and Pr. Gordon Tollin and Dr. John Hurley from the University of Tucson in the United States for their outstanding work in the field and for stimulating collaborations. This work was supported by the CEA, the CNRS, and a grant (R.M.) from the Ministère de l'Education Nationale, de la Recherche et de la Technologie.

Appendix

This appendix aims at illustrating our approach to the electron-transfer problem, as well as showing that we encounter the case of a physical mixing in **I**, for which D will stand as the $[Fe_4S_4(SH)_4]^{3-}$ anion and the acceptor A will be the neutral phenyl group $[C_6H_6]^0$. As it turns out, both molecular orbitals Ψ_+ and Ψ_- are quasi-degenerate, with $\Delta \approx 0$ ($S_{DA} \approx 0$). We therefore encountered severe convergence problems (having interacting orbitals actually helps the convergence). We introduced HOMO mixing, ascribing fractional occupations to the molecular orbitals in order to obtain convergence (cf. section II.3). Again, we thus do not obtain a "real" state though, but rather a mixed state of two states that are individually unreachable (at least in all our attempts to converge them) by the usual DFT means.

It then appears that the reducing electron has been almost equally split among the two $\Psi_+ \approx \Phi_D$ and $\Psi_- \approx \Phi_A$ orbitals in the mixed "rd" state (physical mixing). There is thus no transfer possible from D to A, as is obviously expected when one considers the smallness of the (SH) ligands as well as the distance between both molecules (~8.22 Å between their respective geometrical centers).

We then computed the excited states "ex30" and "ex21" (see Table 2a) defined by $(\Psi_+)^1(\Psi_-)^0$ and $(\Psi_+)^0(\Psi_-)^1$, respectively. Without Phe ring, there is a slight energy gain in locating the extra "reducing" electron on Fe_1 (calculated bonding energy −39.676 eV of the electronic state "rd1") rather than on Fe_2 (−39.562 eV). This can be related to the slight expansion of the coordination sphere around Fe_1, which better accommodates an extra electron in the Fe site, as reduction naturally increases the Fe−S distances.

We also *separately* converged the $[Fe_2S_2(SH)_4]^QD$ and $[Phe65]^QA$ anions ($Q_D + Q_A = -3$), affecting to them fractional charges $-3 < Q_D < -2$ to the former one, $-1 < Q_A < 0$ to the latter one. We then computed (within the point−dipole approximation) the electrostatic repulsion energy R between the two corresponding (Mulliken) charge distributions, defined as

$$R \equiv K \sum_{\substack{i \in D \\ j \in A}} \frac{q_D^i}{r_{ij}}$$

with R in eV, r_{ij} in Å, and $K = 14.4$ eV (conversion factor).

(34) Piubelli, L.; Aliverti, A.; Bellintani, F.; Zanetti, G. *Eur. J. Biochem.* **1996**, *226*, 465−469.
(35) Hirasawa, M.; Hurley, J. K.; Salamon, Z.; Tollin, G.; Markley, J. L.; Cheng, H.; Xia, B.; Knaff, D. B. *Biochim. Biophys. Acta* **1998**, *1363*, 134−46.
(36) Garcia-Sanchez, M. I.; Diaz-Quintana, A.; Gotor, C.; Jacquot, J. P.; DelaRosa, M. A.; Rosa, J. M. *J. Biol. Inorg. Chem.* **2000**, *5*, 713−719.
(37) Schmitz, S.; Böhme, H. *Biochim. Biophys. Acta* **1995**, *1231*, 335−341.
(38) Jacquot, J. P.; Stein, M.; Suzuki, A.; Liottet, S.; Sandoz, G.; Miginiac-Maslow, M. *FEBS Lett.* **1997**, *400*, 293−296.
(39) Müller, A.; Müller, J. J.; Müller, Y. A.; Uhlmann, H.; Bernhardt, R.; Heinemann, U. *Structure* **1998**, *6*, 269−280.
(40) Hoover, D. M.; Drennan, C. L.; Metzger, A. L.; Osborne, C.; Weber, C. H.; Pattridge, K. A.; Ludwig, M. L. *J. Mol. Biol.* **1999**, *294*, 725−743.
(41) Kraulis, P. J. *J. Appl. Crystallogr.* **1991**, *24*, 946−950.
(42) Merritt, E. A.; Bacon, D. *Methods Enzymol.* **1997**, *277*, 505−524.
(43) Rypniewski, W. R.; Breiter, D. R.; Benning, M. M.; Wesenberg, G.; Oh, B.; Markley, J. L.; Rayment, I.; Holden, H. M. *Biochemistry* **1991**, *30*, 4126−31.
(44) Hurley, J. K.; Fillat, M.; Gómez-Moreno, C.; Tollin, G. *Biochimie* **1995**, *77*, 539−548.
(45) Hurley, J. K.; Caffrey, M. S.; Markley, J. L.; Cheng, H.; Xia, B.; Chae, Y.-K.; Holden, H. M.; Tollin, G. *Protein Sci.* **1995**, *4*, 58−64.

For example, the case of two punctual charges $Q_D = \sum_i q_d^i = -2$ and $Q_A = \sum_j q_A^j = -1$ separated by $r = 8.22$ Å yields a value of $R = 3.5$ eV. As a consequence, if the D and A molecules are effectively not interacting, one can expects the R values for both "ex21" and "ex30" to reflect it by being close to 3.5 and 0.0 eV, respectively. Moreover, the sum of the bonding energies of the isolated molecules $E_D + E_A$ corrected by the corresponding R value should equate rather well that of the combined [D−A] system. This would not be true in the case of interacting D and A molecules, with partially delocalized charges. It can be seen from Table 4 that the R values range from −0.08 to 3.25 eV and that there is a minimum energy for $E_D + E_A + R$ for $Q_D = Q_A = 0.5$. We verified moreover that the charge distributions obtained for the isolated $[Fe_2S_2(SH)_4]^{2.5-}$ and $[Phe65]^{-0.5}$ anions, as well as for the whole [D−A] mixed system, are indeed very close.

JA011680O